Available online at www.sciencedirect.com
ScienceDirect
Journal of Photochemistry and Photobiology A: Chemistry 197 (2008) 177–189
Journal of Photochemistry and Photobiology A:Chemistry
www.elsevier.com/locate/jphotochem

# Abatement of volatile organic compounds using an annular photocatalytic reactor: Study of gaseous acetone

G. Vincent, P.M. Marquaire, O. Zahraa *

*Département de Chimie Physique des Réactions, UMR 7630 CNRS, Nancy-Université, ENSIC, 1 rue Grandville, BP 20451, 54001 Nancy Cedex, France*

Received 5 July 2007; received in revised form 19 December 2007; accepted 26 December 2007
Available online 5 January 2008

**Abstract**

Photocatalytic oxidation of organic compounds in gas phase appears to be a promising process for remediation of polluted air. In the present work, the photocatalytic degradation of acetone, which is a typical pollutant of indoor air, was investigated by using an annular photoreactor. After a modelling by a cascade of elementary continuously stirred tank reactor, the annular photoreactor was assimilated to a plug flow reactor (PFR). No transfer limitation (external and internal) has been demonstrated for this reactor with the fibreglass photocatalytic support. The influence of several kinetic parameters has been studied such as pollutant concentration, incident light irradiance, contact time and humidity content. The Langmuir–Hinshelwood model has been verified for acetone. It can be noticed that no by-products have been detected by FID suggesting almost total mineralization. The possible minor gaseous by-products have been accumulated into a mixture of ethanol–liquid nitrogen at −50 °C then a sample of it has been injected into a GC/MS for analysis. A mechanistic pathway is then proposed for the photocatalytic degradation of acetone.


*Keywords:* Annular reactor; Radiation field; Kinetic modelling; By-products; Photocatalytic degradation mechanism

## 1. Introduction

Photocatalytic oxidation of airborne contaminants appears to be a promising process for remediation of air polluted by volatile organic compounds (VOCs) or by bacteria [1]. VOCs are well known to be malodorous, toxic and some of them can be considered as carcinogenic, mutagenic and teratogenic. There are a number of available photocatalytic reactor configurations for the abatement of airborne pollutants: (1) flat plate fluidized bed reactor, (2) fluidized bed reactor, (3) fixed layer photocatalytic reactor, (4) photocatalytic reactor with fibre optic bundles, and (5) annular photocatalytic reactor [2]. This annular geometry is widely used for controlling VOC emissions in indoor air. A large diversity of reactor configurations has been considered to study the efficiency of photocatalytic degradation of air pollutants. Photocatalytic reactors require several of important reactor parameters such as [2,3]:

- UV source;
- reactor configuration;
- catalyst type, distribution and impregnation;
- interaction between the light, catalyst and reacting flowing.

This work focuses on the photocatalytic degradation of acetone. *Natural pollution sources*: acetone is mainly produced via oxidation of humic substances and it occurs naturally as a metabolic by-product of plants and animals. *Artificial pollution sources*: acetone is widely used as solvent for fats, oils, waxes, resins, rubbers, plastics and pharmaceuticals. Indoor air, the presence of acetone is due to the use of domestic materials and products as paints and cleaning products. Acetone was detected at concentrations between 14.9 ng $L^{-1}$ (35.8 ppb) and 66.0 ng $L^{-1}$ (158.4 ppb) at dwelling houses. This ketone has a threshold limit value (TLV) in air of 1.2 mg $L^{-1}$ (500 ppm) [4]. The threshold limit value is the maximum permissible concentration of a pollutant generally defined in workplace atmospheres. Our photocatalytic reactor could be used to reduce VOC emissions in workplace atmospheres or in dwelling house indoor air.

* Corresponding author. Fax: +33 3 83 37 81 20.
*E-mail address:* Orfan.Zahraa@ensic.inpl-nancy.fr (O. Zahraa).

1010-6030/$ – see front matter © 2008 Elsevier B.V. All rights reserved.
doi:10.1016/j.jphotochem.2007.12.021

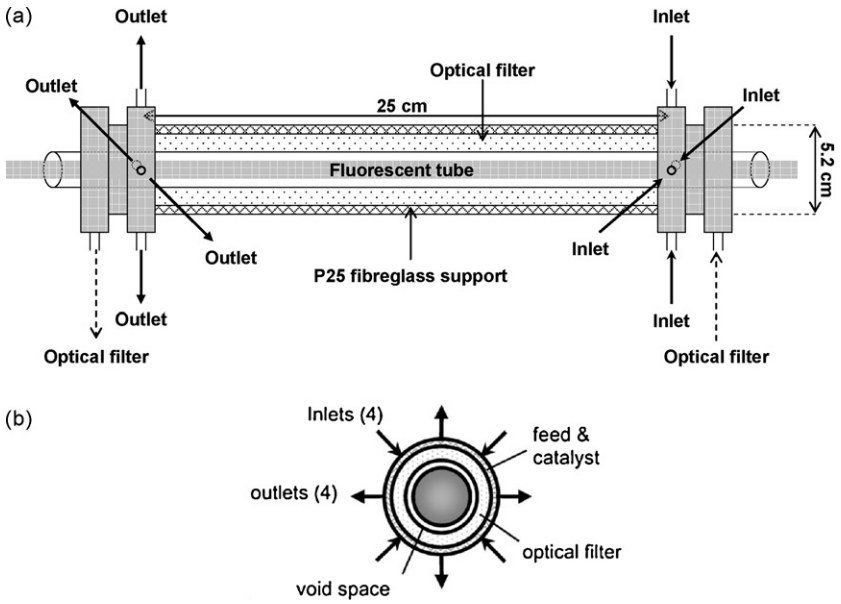


Fig. 1. Schematic representation (a) and sectional drawing (b) of the annular photoreactor.

The first part of this work deals with the results of the acetone kinetic study. Our annular photocatalytic reactor was modelled by a cascade of continuously stirred tank reactors (CSTRs) in order to classify the category of reactor. The second part of this work consists in summarizing the study of by-products, which were formed during the photocatalytic degradation of acetone. A mechanistic pathway was proposed for its photocatalytic degradation.

## 2. Experimental

### 2.1. Experimental set-up and procedure

The annular photocatalytic reactor was equipped with four inlets and four outlets in order to ensure a good flow distribution (Fig. 1). A fibreglass support (effective porosity $\varepsilon = 0.95$) impregnated of $TiO_2$ Degussa P25 was inserted between two Pyrex glass tubes with a thickness of 1.8 mm. This low thickness provides a best contact between polluted air and photocatalyst. A commercial Philips® TLD 18 W/08 fluorescent tube is placed in the centre of the unit offering the best conditions of light irradiance. It can be noticed that the UV lamp has a spectral peak centred at about 365 nm. In a previous work, the 3-W light power has been verified by actinometry [5]. The fluorescent tube and the photocatalyst were separated by a liquid filter in order to control both temperature and light irradiance during the degradation process. The light transmission was attenuated by a specific nigrosine concentration in aqueous solution. The total diameter, the volume and the photoactive length of the annular reactor were, respectively 5.2 cm, 66.4 $cm^3$ and 25 cm. The diameter of the space for the fluorescent tube was 30.5 mm. The thickness available for the photocatalyst support was about 1.8 mm. The fibreglass support apparent area exposed to UV was 300 $cm^2$. The experimental unit permits to generate a polluted air with a specific VOC concentration and humidity content. The functioning of the experimental set-up has been widely detailed in previous works [5,6]. Several kinetic parameters can be tested on the photocatalytic degradation efficiency as initial concentration of pollutant, light irradiance, contact time and humidity content.

A gas chromatograph equipped with a flame ionization detector (FID) was used to follow acetone concentration during photocatalytic oxidation. For this pollutant, the response of the FID was linear and proportional to the amount of acetone. Finally the acetone conversion $X$ in the reactor is expressed by the following equation:

$$X = 1 - \frac{C_{out}}{C_{in}} = 1 - \frac{A_{out}}{A_{in}} \quad (1)$$

The GC is a Hewlett Packard 5890 Series II apparatus equipped with a FID. The GC operational parameters were as follows: analytical column, Porapak Q column 1/8 in. (1 m) at 180 °C; carrier gas, nitrogen at 21 mL $min^{-1}$; injected volume, 1 $cm^3$; FID detector at 250 °C supplied with air/hydrogen at 276 and 38 mL $min^{-1}$, respectively.

The by-products generated during the photocatalytic degradation of acetone were identified by GC/MS. The GC/MS is an Agilent 6850 Series apparatus equipped with a mass selective detector (MSD) Agilent 5973 Network. The GC/MS operational parameters were as follows: analytical column, HP Plot Q (30 m × 0.32 mm i.d.); carrier gas, helium at 1.5 mL $min^{-1}$; program temperature, 40 °C for 10 min, 5 °C $min^{-1}$ and 240 °C 10 min; temperature of injector, 250 °C (split = 4.5 mL $min^{-1}$); injected volume, 1 μL; detector, MSD at 250 °C.

### 2.2. Catalyst preparation

The catalyst consisted of $TiO_2$ P25 Degussa deposited on a Sintomat® fibreglass support (250 mm × 120 mm). A single

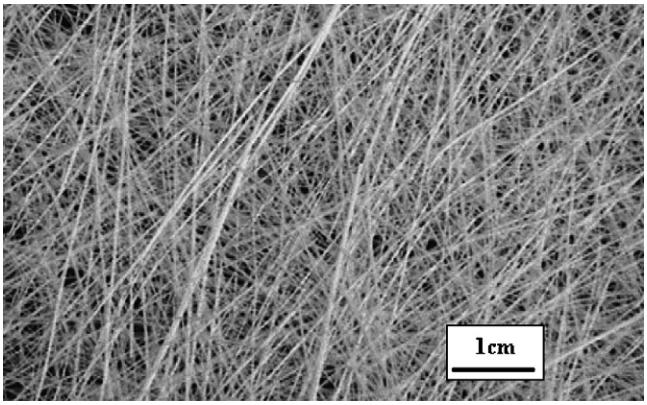


Fig. 2. Optical picture of fibreglass photocatalytic support.

rectangular section of fibreglass support (300 $cm^2$) was inserted inside the photoreactor. From Fig. 2, the fibreglass support is like a mat of thickness 1.8 mm, where fibre bundles of rectangular section 300 μm × 400 μm are randomly oriented. The catalyst deposition followed a specific protocol more detailed in a previous work [7]. $TiO_2$ P25 Degussa was dispersed in an aqueous suspension adjusted at pH 3 with nitric acid in order to prevent the titanium dioxide aggregation. The fibreglass support was impregnated with this suspension. After complete evaporation of water, the support was dried at 100 °C for 1 h and fired at 475 °C for 4 h to ensure a good adherence between catalyst and support. About 600 mg of $TiO_2$ was deposited on fibreglass support.

### 2.3. Fluorescent tube modelling

In general, all of the existing light distribution models are classified into two different categories: line source models and extensive source models. In line source models, the light source is assimilated to a line, whereas in extensive source models, dimensions of the lamp are considered [8,9]. Therefore, in the extensive source models, the characteristics of the lamps can be used as design parameters of the photoreactors. In this present work, we have developed a Lambert extensive source model (LESM) to predict the light distribution of the fluorescent tube. This extensive model is the most complex but it is more realistic.

#### 2.3.1. Emission law

The fluorescent tube can be assimilated to a cylindrical area where each surface element $dS_L = dz_L R\, d\varphi_G$ emits in a half space via the Lambert's law as below (Fig. 3):

$$d^2F = L_T(\theta_e, \varphi_e) dS_L d\Omega_e \quad (2)$$

where the target element has the angular coordinates $\theta_e$ and $\varphi_e$ compared to a local axis system at emitting point: $\varphi_e$ rotation of MN normal to $dS_L$ around Mz′ generator giving MN′ and $\theta_e$ which is the angle compared with MN′ in the (Mz′, MN′) plan. The element corresponding to $d\theta_e$ and $d\varphi_e$ is the solid angle $d\Omega_e = \cos\theta_e\, d\theta_e\, d\varphi_e$. From the Lambert's law, the term $\cos\theta_e \cos\varphi_e$ is the cosine of the emitting angle with the MN normal and it follows for the luminance $L_T$:

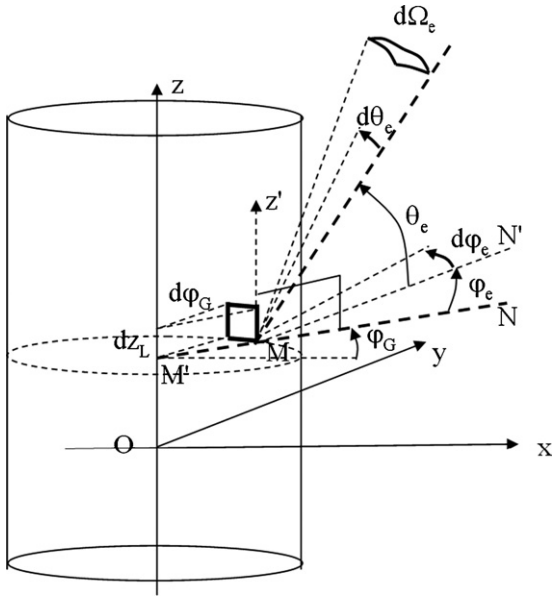


Fig. 3. Geometry for the emission model. $dS_L$ is characterized by the bold square with $dS_L = dz_L R\, d\varphi_G$ where $R$ represents the fluorescent tube radius. $\varphi_e$ rotation of MN normal to $dS_L$ around Mz′ generator giving MN′ and $\theta_e$ which is the angle compared with MN′ in the (Mz′, MN′) plan. The solid angle $d\Omega_e$ is defined by: $d\Omega_e = \cos\theta_e\, d\theta_e\, d\varphi_e$.

$$L_T(\theta_e, \varphi_e) = L'_T \cos\theta_e \cos\varphi_e \quad (3)$$

The integration of $L'_T \cos\theta_e \cos\varphi_e d\Omega_e = L'_T \cos^2\theta_e d\theta_e \cos\varphi_e d\varphi_e$ on the whole half space, with $(-\pi/2, +\pi/2)$ for $\varphi_e$ and $(-\pi/2, +\pi/2)$ for $\theta_e$, gives $L'_T(\pi/2)(2)$. Therefore, the integration on the whole emitting area is given as follows:

$$F^\circ = (2\pi RZ)L'_T(\pi) \Rightarrow L'_T = \frac{F^\circ}{2\pi^2 ZR} \quad (4)$$

where $F^\circ$ is the total light power of the fluorescent tube (W), $Z$ the total length of the fluorescent tube from $-Z/2$ to $+Z/2$ (cm) and $R$ is the fluorescent tube radius (cm). Therefore, the emitting law is written as below:

$$d^2F = \frac{F^\circ}{2\pi^2 ZR} dS_L \cos\theta_e \cos\varphi_e\, d\Omega_e \quad (5)$$

#### 2.3.2. Light irradiance model

The light irradiance is established for a target point C at given distances $z_C$, $r_C$ on a surface element $dS_C$, which belongs to $O_z$-axis cylinder and going trough C. Where $z_C$ is the axial distance (cm) and $r_C$, the radial distance (cm). The emitting law at C point is as follows (Fig. 4):

$$d^2F = \frac{F^\circ}{2\pi^2 ZR} dS_L \cos\theta_e \cos\varphi_e\, d\Omega_C \quad \text{with } dS_L = R dz_L\, d\varphi_G \quad (6)$$

The calculus of $d\Omega_C$ is given as below:

$$d\Omega_C = \frac{dS_C \cos(N_C, CM)}{MC^2} \quad (7)$$

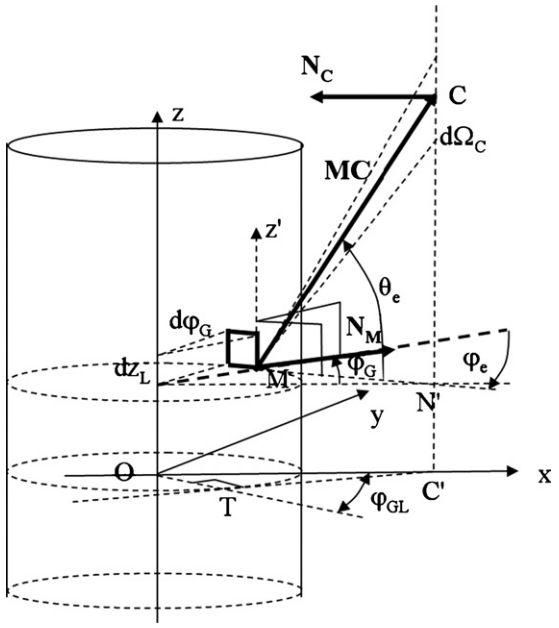


Fig. 4. Geometry for the light irradiance model. The incident light irradiance is established for a target point C at given distances $z_C$, $r_C$ on a surface element $dS_C$, which belongs to $O_z$ axis cylinder and going through $C$. Where $z_C$ is the axial distance and $r_C$, the radial distance. $dS_L$ is characterized by the bold square with $dS_L = dz_L R\, d\varphi_G$ where $R$ represents the fluorescent tube radius. The solid angle $d\Omega_C$ is defined by: $d\Omega_C = dS_C \cos(N_C, CM)/MC^2$.

where $N_C$ is the normal to $dS_C$. The coordinates of $M$, $C$, CM and $N_C$ are given as follows:

$$M(R\cos\varphi_G,\ R\sin\varphi_G,\ z_L)$$
$$C(r_C,\ 0,\ z_C)$$
$$CM[(R\cos\varphi_G - r_C),\ R\sin\varphi_G,\ (z_L - z_C)]$$
$$N_C(-1,\ 0,\ 0)$$

$$\cos(N_C, CM) = -\frac{(R\cos\varphi_G - r_C)}{MC} \quad \text{with } MC^2$$
$$= (R\cos\varphi_G - r_C)^2 + (R\sin\varphi_G)^2 + (z_L - z_C)^2 \tag{8}$$

The calculus of $\cos\theta_e \cos\varphi_e$ is established as below. It can be noticed that $\cos\theta_e \cos\varphi_e$ corresponds to $\cos(N_M, MC)$ which is the angle cosine between the normal to $dS_L$, $N_M$ and the $MC$ emitting direction:

$$N_M(\cos\varphi_G,\ \sin\varphi_G,\ 0)$$
$$\cos(N_M, MC) = \frac{-\cos\varphi_G(R\cos\varphi_G - r_C) - \sin\varphi_G(R\sin\varphi_G)}{MC}$$
$$\cos(N_M, MC) = \frac{r_C\cos\varphi_G - R}{MC} \tag{9}$$

The incident light irradiance $I_0$ is given as below:

$$d^2 I_0 = \frac{d^2 F}{dS_C} = \left[\frac{F^\circ}{2\pi^2 ZR}\right][R\, dz_L\, d\varphi_G]\cos(N_M, MC)$$
$$\frac{dS_C \cos(N_C, CM)/MC^2}{dS_C} \tag{10}$$

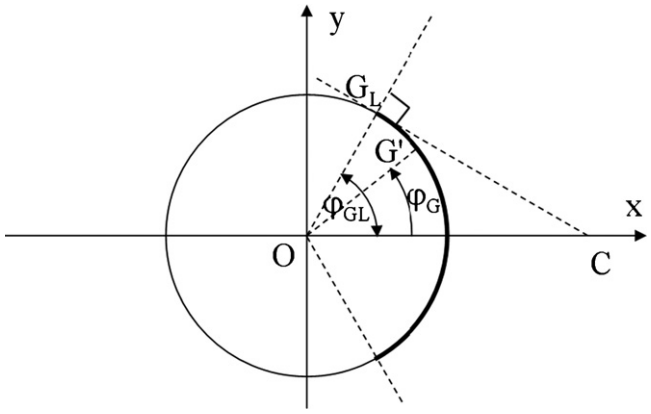


Fig. 5. Geometry for the limit value of $\varphi_G$.

$$d^2 I_0 = \left[\frac{F^\circ}{2\pi^2 Z}\right][dz_L d\varphi_G][r_C\cos\varphi_G - R]\frac{r_C - R\cos\varphi_G}{MC^4} \tag{11}$$

The calculus of incident light irradiance in C has been realised by a numerical integration of $d^2 I_0$ with: $z_L$ $(-Z/2, +Z/2)$ and $\varphi_G$ $(-\varphi_{GL}, +\varphi_{GL})$. The limit value of $\varphi_G$, as illustrated in Fig. 5, is defined by the following equation:

$$\varphi_{GL} = \cos^{-1}\left(\frac{OG_L}{OC}\right) = \cos^{-1}\left(\frac{R}{r_C}\right) \tag{12}$$

$$I_0(r_C, z_C) = \left[\frac{F^\circ}{2\pi^2 Z}\right]\int_{-\varphi_{GL}}^{+\varphi_{GL}}\int_{-Z/2}^{+Z/2} \times \frac{(r_C\cos\varphi_G - R)(r_C - R\cos\varphi_G)}{\left[(R\cos\varphi_G - r_C)^2 + (R\sin\varphi_G)^2 + (z_L - z_C)^2\right]^2} dz_L d\varphi_G \tag{13}$$

It can be noticed that the incident light irradiance model predicts only the light distribution for a fluorescent tube. The target point C can be located on the internal reactor wall but not inside the photocatalytic bed. The reflected, absorbed and transmitted light fractions on a $TiO_2$ flat plate can be easily determined, using a spectrophotometer equipped with an integrated sphere. This technique has been well detailed in a previous work [10]. However, the absorption and scattering properties of $TiO_2$ deposited on fibreglass could not be measured by spectrophotometry due to the non-homogeneous nature of support. Therefore, the radiation absorption and scattering are not taken into account. It can be noticed that the Pyrex absorption is insignificant for this wavelength (365 nm) and the light transmission is almost total. The axial and radial distribution experiments were investigated, respectively at different axial and radial positions using an UV-sensitive radiometer (VLX-365). The total light power ($F^\circ$) has been assimilated to 3 W as described in a previous work [5]. The axial distribution of the light irradiance was investigated in the range of 0–50 cm. It can be observed from Fig. 6 that experimental data seem to be well fitted by the simulated results predicted by the LESM. Here we show that the light irradiance is relatively constant as far as $z_C = 20$ cm (constant from −20 to +20 cm). It can be noticed that the annular reactor has a 25-cm photoactive

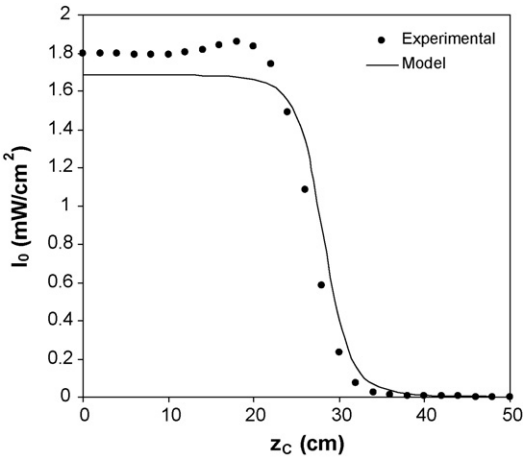


Fig. 6. Axial distribution for the fluorescent tube ($r_C = 5$ cm).

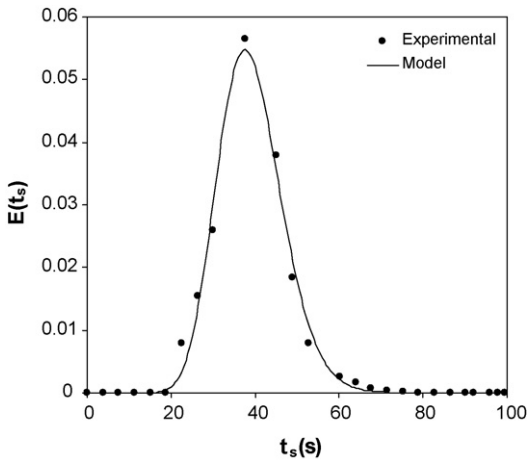


Fig. 8. Residence time distribution $E(t_s)$ of the annular photoreactor, $J = 26$.

length, where the light irradiance is stable and constant. The radial distribution of the light irradiance was investigated in the range of 5–20 cm. Fig. 7 indicates that the simulated results predicted by the LESM agreed well with the experimental data. Here we can see that the light irradiance decreases as the radial position increases from 5 to 20 cm.

## 3. Photocatalytic results and discussion

### 3.1. Annular photoreactor modelling

It is evident that elements of fluid taking different routes through the reactor may take different lengths of time to pas through the vessel. The distribution of these times for the stream of fluid leaving the vessel is called the residence time distribution (RTD) of fluid. Experiments of RTD were carried out using a pulse of hydrogen in the feed detected at the photoreactor exit by a thermal conductivity detector (TCD). To simulate a pulse function (Dirac function), a tracer substance (hydrogen) was injected during a very short time interval into the reactor. The RTD $E(t_s)$ is expressed as a function of time ($t_s$) by the following equation [11]:

$$E(t_s) = \frac{C(t_s)}{\int_0^\infty C(t_s)\mathrm{d}t_s} \cong \frac{y(t_s)}{\sum_0^n y(t_s)\Delta t_s} \quad (14)$$

where $C(t_s)$ is the tracer concentration at the reactor output; $y(t_s)$ the response of the detector and $n$ is the total number of performed measurements. The tanks in series model describe systems with a complete mixture like the ideally stirred tank reactor ($J = 1$) or the ideal cascade of continuously stirred tank reactors ($J > 1$). It is generally accepted that above a number of 20 elementary reactors, the used reactor can be considered practically as a plug flow reactor. The experiments of RTD revealed that our annular reactor could be assimilated to a cascade of 26 elementary continuously stirred tank reactor ($J = 26$) close to a plug flow reactor (PFR) (Fig. 8). In a previous study, $J = 18$ has been found with the same reactor but with another packed catalyst [6].

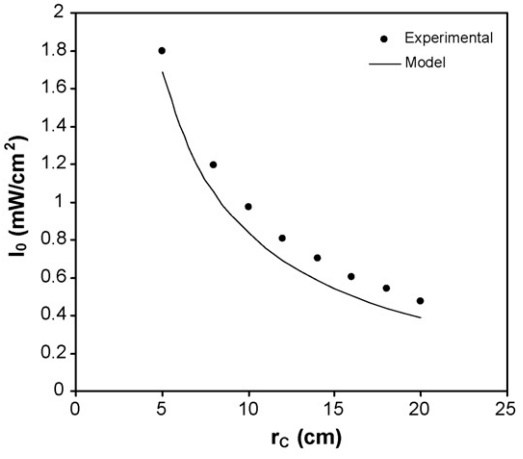


Fig. 7. Radial distribution for the fluorescent tube ($z_C = 0$).

### 3.2. External and internal mass transfer

Mass transfer phenomena can be classified as external, within the fluid in the vicinity of the catalyst pellets or deposits, and as internal within the catalyst pores. The rate of external mass transfer ($N_D$) is generally expressed according to the model of the boundary layer on the catalyst surface via the expression as below [3]:

$$N_D = k_D(C_b - C_s) \quad (15)$$

where $C_b$ is the bulk concentration and $C_s$ the surface concentration. The rate constant $k_D$ depends on the flow regime of the fluid, characterized by the dimensionless Reynolds number $Re$ via the following empirical expression [3,12]:

$$k_D = 3.49 \times 10^{-7}\, Re^{0.77} \quad (16)$$

The rate constant $k_D$ increases parallely with the flow turbulence. Therefore, a good stirring is necessary to prevent an external mass transfer. When the mass transfer influence is significant, the degradation rate of the pollutant increases parallely with the flow rate. The effect of external mass transfer of the cat-

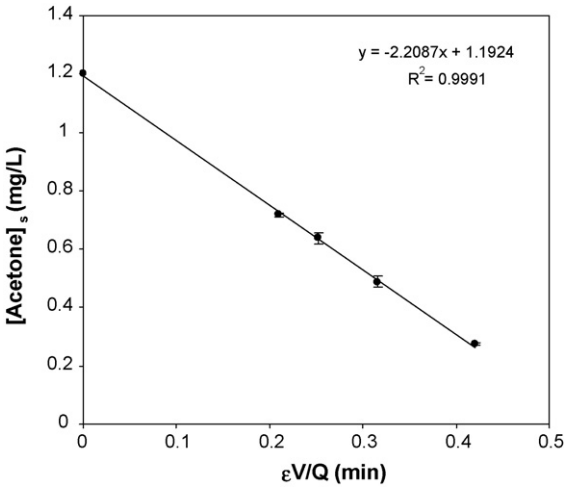


Fig. 9. Effect of the total flow rate on the rate of degradation. Regular conditions used were: incident light irradiance, $\bar{I}_0 = 1.7\,\mathrm{mW\,cm^{-2}}$; relative humidity, RH = 10%; photoreactor temperature, $T_R = 30\,^{\circ}\mathrm{C}$; initial concentration, $C_0 = 1.2\,\mathrm{mg\,L^{-1}}$; oxygen content, air (20 vol% $O_2$).

alyst was investigated using different flow rates of the gas $Q_v$ ranging from 150 to 300 mL min$^{-1}$. It can be noticed that the rate is expressed per unit of reactor apparent volume. In a PFR, the rate of disappearance of acetone is defined by the following expression:

$$r = -\frac{\mathrm{d[Acetone]_s}}{\mathrm{d}(\varepsilon V/Q_v)} \tag{17}$$

with

$$\varepsilon = \frac{\text{volume occupied by the flowing fluid}}{\text{total volume of photoreactor}} = \frac{Q_v}{V}\overline{t_s} \tag{18}$$

where $r$ is the apparent rate of disappearance of acetone; [Acetone]$_s$ the outlet concentration of acetone; $Q_v$ the volumetric flow rate; $\varepsilon$ the effective porosity and $V$ is the total volume of photoreactor. In the absence of an external mass transfer limitation, the reaction rate in a fixed bed reactor does not depend on the volumetric flow rate. From Fig. 9, the apparent rate of disappearance of acetone is directly obtained with the slope of the straight line. No significant differences in the degradation rate were observed under experimental conditions with the variation of volumetric flow rate studied. Therefore, the reaction rate was not kinetically limited by the external mass transfer. The fibreglass photocatalytic support allows preventing an external mass transfer due to a turbulent flow in this annular geometry.

The presence of a kinetic limitation by internal mass transfer could be evaluated using the non-dimensional Weisz modulus $\varphi'$, which is a modified of the Thiele modulus. The Weisz modulus $\varphi'$ is only based on observable parameters and its expression is given by the following equation [3,12]:

$$\varphi' = \frac{\bar{r}L^2}{D_e C_s} \quad \text{with} \quad D_e = \frac{\varepsilon_p D}{\tau_p} \tag{19}$$

where $\bar{r}$ is the experimental mean rate of reaction per unit of catalyst; $L$ the characteristic dimension of the deposit; $D_e$ the effective diffusion coefficient of VOC within the porous solid; $D$ the diffusion coefficient of VOC in air; $\varepsilon_p$ the catalyst grain porosity ($\varepsilon_p$ about 0.5 for $TiO_2$ Degussa P25); $\tau_p$ the pore tortuosity (about 3 [5]) and $C_s$ is the mean surface concentration (equal to the mean concentration in the reactor due to the absence of external mass limitation). A previous study has showed that the catalyst on fibreglass support was consisted of $TiO_2$ isolated aggregates of diameter of about 5–10 μm [5]. Under the most severe conditions, a maximum diameter of 5 μm for the catalyst grain was chosen for the characteristic dimension of the deposit. The diffusion coefficient in air for acetone has been evaluated to $9.42 \times 10^{-6}\,\mathrm{m^2\,s^{-1}}$. After calculation $\varphi'$ was estimated to about $5.7 \times 10^{-6}$ for the photocatalytic degradation of acetone in the annular reactor. It is generally assumed that an internal mass limitation occurs when $\varphi' \gg 1$. Therefore, it could be considered that there was no kinetic limitation by internal mass transfer due to the low value determined $\varphi' \ll 1$.

### 3.3. Effect of the acetone concentration

The effect of initial pollutant concentration $C_0$ on the photocatalytic degradation rate was investigated in the range of 0.29–1.73 mg L$^{-1}$. In photocatalytic studies, kinetics of photodegradation are generally represented by the Langmuir–Hinshelwood (LH) model. The reaction rate ($r$) is defined by the following relationship [13]:

$$r = k_{deg}\frac{K_{LH}C}{1 + K_{LH}C} \tag{20}$$

where $K_{LH}$ is the adsorption constant (L mg$^{-1}$); $C$ the concentration of acetone in the gas-phase (mg L$^{-1}$) and $k_{deg}$ an apparent kinetic constant (mg min$^{-1}$ L$^{-1}$). It can be noticed that the rate is expressed per unit of reactor apparent volume. The importance of substrate preadsorption on a given photocatalyst can be evaluated by the use of an LH kinetic model, considering that the adsorption of reaction intermediates and products is not significant. In our case, no by-products were detected by the FID during the photocatalytic process. Previously our annular reactor has been assimilated to a cascade of 26 elementary continuously stirred tank reactors ($J = 26$) close to a PFR. Therefore, the mass balance through the annular photoreactor is given by the following equation:

$$-\frac{\mathrm{d}C}{\mathrm{d}(\varepsilon V/Q_v)} = k_{deg}\frac{K_{LH}C}{1 + K_{LH}C} \tag{21}$$

where $V$ is the total volume of photoreactor; $Q_v$ the volumetric flow rate and $\varepsilon$ is the effective porosity. The integration of Eq. (21) is possible only when there is no limitation by mass transfer: no difference of concentration between bulk flow and the catalyst surface. By integrating and rearranging Eq. (21), it follows:

$$\frac{1}{k_{deg}K_{LH}}\ln\left(\frac{C_{out}}{C_0}\right) + \frac{1}{k_{deg}}(C_{out} - C_0) = -\varepsilon\frac{V}{Q_v} \tag{22}$$

Eq. (22) can be written introducing the pollutant conversion $X = 1 - C_{out}/C_0$:

$$\frac{1}{k_{deg}K_{LH}}\ln\left(\frac{1}{1 - X}\right) + \frac{1}{k_{deg}}(C_0 X) = \varepsilon\frac{V}{Q_v} \tag{23}$$

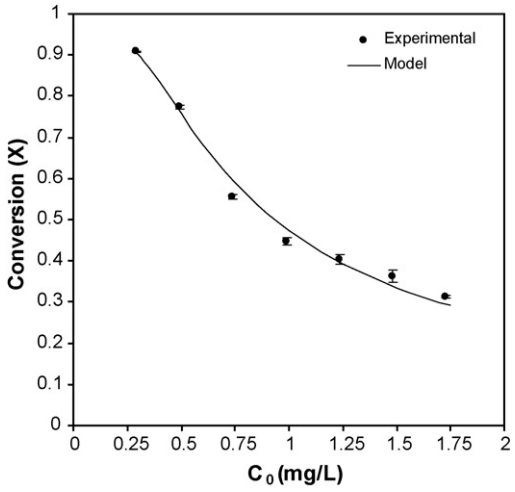


Fig. 10. Effect of the initial concentration on the acetone conversion. Regular conditions used were: total volume flow rate, $Q_v = 300\,mL\,min^{-1}$; relative humidity, RH = 10%; photoreactor temperature, $T_R = 30\,^{\circ}C$; incident light irradiance, $\bar{I}_0 = 1.7\,mW\,cm^{-2}$; oxygen content, air (20 vol% $O_2$).

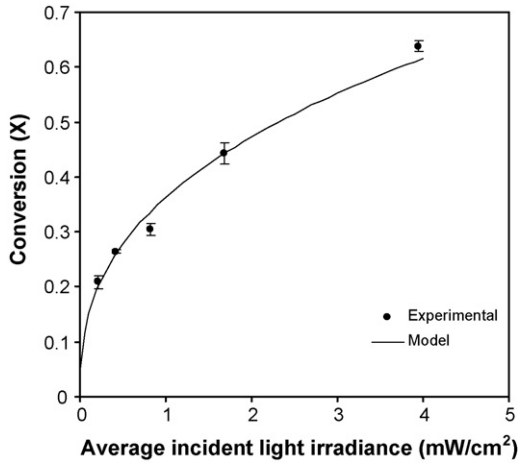


Fig. 11. Effect of the average incident light irradiance on the acetone conversion. Regular conditions used were: total volume flow rate, $Q_v = 300\,mL\,min^{-1}$; relative humidity, RH = 10%; photoreactor temperature, $T_R = 30\,^{\circ}C$; initial concentration, $C_0 = 1.2\,mg\,L^{-1}$; oxygen content, air (20 vol% $O_2$).

A plot of $-\varepsilon V/Q_v C_0 X$ vs. $\ln(1–X)/(C_0 X)$ should be linear and will allow the two constants $k_{deg}$ and $K_{LH}$ to be determined. From this optimization, the values of $k_{deg}$ and $K_{LH}$ obtained are, respectively $2.63\,mg\,min^{-1}\,L^{-1}$ and $8.16\,L\,mg^{-1}$. It is possible for a given inlet concentration to determine the pollutant conversion by solving Eq. (23). The effect of the acetone concentration is shown in Fig. 10. At low adsorption or low concentration, $r$ is equal to $k_{deg}K_{LH}C$ (first-order kinetic) and at high adsorption or high concentration, $r$ is equal to $k_{deg}$ (zero-order kinetic). This behaviour is in agreement with the LH model proposed by Kim and Hong [14].

### 3.4. Effect of the incident light irradiance

The effect of the incident light irradiance on the photocatalytic degradation of acetone was investigated in the range of 0.21–3.94 mW cm$^{-2}$. The light transmission was attenuated by a nigrosine solution in the temperature-regulated bath. From Wang et al. [15], the kinetic constant is a function of light irradiance as below:

$$k_{deg} = k'' I_0^n \tag{24}$$

where $k''$ is a rate constant independent of incident light irradiance; $I_0$ the incident light irradiance and $n$ is the kinetic order with respect to $I_0$. Therefore, the mass balance through the annular photoreactor is given by the following equation:

$$-\frac{dC}{d(\varepsilon V/Q_v)} = k'' I_0^n \theta \quad \text{with} \quad \theta = \frac{K_{LH}C}{1 + K_{LH}C} \tag{25}$$

The incident light irradiance has been measured by an UV-sensible radiometer (VLX-365). As described previously, the absorption and scattering light inside the photocatalytic bed are not taken into account due to a non-homogeneous support. Therefore, the model of light distribution allows estimating the incident light irradiance reaching the surface of photocatalytic support. In first approximation, we have only considered that the reaction took place on the surface of photocatalytic support. It can be noticed that the reaction takes place in the whole reactor volume but the constraints of fibreglass support and its non-homogeneous nature prevent the modification of the light irradiance model. The incident light irradiance is relatively constant on the photoactive length of reactor but an average value should be considered as the employed light irradiance model gives a local value:

$$\bar{I}_0(r_C) = \frac{\int_{-L/2}^{+L/2} I_0(r_C, z)dz}{L} \exp(-\varepsilon d_{app} x) \tag{26}$$

where $\bar{I}_0$ represents an average value of incident light irradiance; $\varepsilon$ a global extinction coefficient of light through the photocatalytic media, which takes into account both absorption and scattering of light; $d_{app}$ the apparent density of photocatalytic support; $x$ the fibreglass thickness; $L$ is the photoactive length of reactor and $-L/2 < z < +L/2$. By integrating and rearranging Eq. (25), it follows:

$$k'' \bar{I}_0^n \theta \varepsilon \frac{V}{Q_v} = C_0 - C_{out} \tag{27}$$

where $\theta$ is the surface coverage of acetone. Eq. (27) can be written introducing the pollutant conversion $X = 1 - C_{out}/C_0$:

$$\bar{I}_0^n \beta = C_0 X \quad \text{with} \quad \beta = k'' \theta \varepsilon \frac{V}{Q_v} \tag{28}$$

A plot of $\ln(C_0 X)$ vs. $\ln(\bar{I}_0)$ should be linear and will allow the two constants $n$ and $\beta$ to be determined. The plot is linear with a slope ($n$), which is equal to 0.38. The effect of the incident light irradiance on the photocatalytic degradation of acetone is shown in Fig. 11. The photodegradation rate of acetone follows linear dependency with $\bar{I}_0^{0.38}$ in the studied range according to

$$r = k'' \bar{I}_0^{0.38} \theta \tag{29}$$

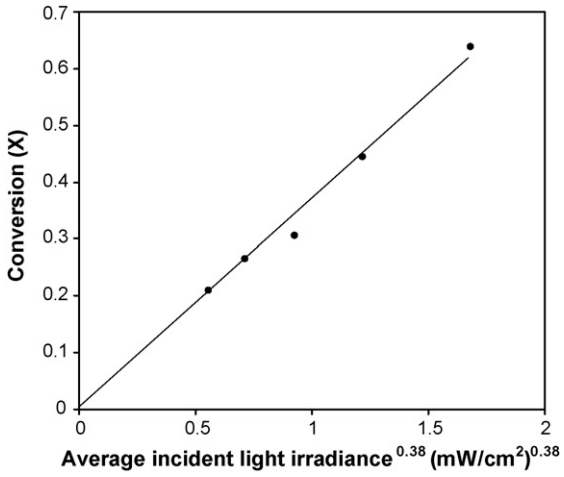


Fig. 12. Representation of $X$ vs. $\bar{I}_0^{0.38}$.

It has been frequently reported that $n$ values range between 0, 0.5 and 1 in various kinds of photocatalytic reactions: $n = 1$ at low light irradiance, $n = 0.5$ at medium light irradiance and $n = 0$ at high light irradiance. In the first-order regime, the electron–hole pairs are consumed more rapidly by chemical reactions than by recombination reactions. In the half-order regime, the rate of electron–hole formation exceeds the rate of photocatalytic oxidation, resulting in electron–hole recombination. In the zero-order regime, the reactions are mass transfer limited [16,17]. The reaction rate could be limited by the external and/or internal mass transfer since the kinetic order $n$ is lower than the half-order ($n = 0.5$). Ohko et al. [18] have mentioned a possible mixed control where the experimental regime was in a transition region between the two asymptotic values (here, $0 < n < 1/2$). In a previous work, Ohko et al. [19] have attributed the formation of a plateau in $r$ vs. $I_{abs}$ (absorbed photon flux) curves to situations where the reactions were limited by the mass transfer. However, in our case, the absence of a plateau in $X$ vs. $\bar{I}_0^{0.38}$ suggests absence of significant external and/or internal mass transfer limitations (Fig. 12). Chen and Chou [20] have studied the photodecolorization of methyl orange using titanium dioxide as catalyst. The chemical reaction was the rate-determining step in this system since both external and internal mass transfer resistances were insignificant. These authors have studied the effect of irradiation intensity and they have observed that the initial reaction rate was proportional to 0.25 order of the light intensity. Recently, Rincón and Pulgarin [21] have mentioned that a non-linear correlation between light intensity and degradation of organic compounds could be due to the fact that excessive $OH^\bullet$ radical generation at high intensity leads to their self-recombination. A recombination between radicals could take place in the photocatalysis process that allows explaining the obtained value, which is lower than the half-order ($n = 0.38$). The following elementary reaction equations have been taken into account:

$$TiO_2 + h\nu \xrightarrow{k_1} e^- + h^+ \quad (30)$$

$$e^- + h^+ \xrightarrow{k_2} \text{heat} \quad (31)$$

$$h^+ + OH^-(H_2O) \xrightarrow{k_3} OH^\bullet(+H^+) \quad (32)$$

$$OH^\bullet + C \xrightarrow{k_4} P \quad (33)$$

$$OH^\bullet + OH^\bullet \xrightarrow{k_5} H_2O_2 \quad (34)$$

Eq. (30) refers to the photonic activation step. Eq. (31) depicts the recombination step between $e^-$ and $h^+$, Eq. (32) represents the formation of hydroxyl radicals, Eq. (33) characterizes the transformation of the organic compound C into product P by $OH^\bullet$ attack and in Eq. (34) the recombination between two hydroxyl radicals is suggested. The photocatalytic degradation rate of the organic compound $r$ is represented by the following expression:

$$r = k_4[OH^\bullet][C] \quad (35)$$

The concentration of photo-induced holes $[h^+]$ can be obtained using the steady state assumption as below:

$$\frac{d[h^+]}{dt} = k_1 I - k_2[h^+]^2 - k_3[h^+][OH^-] \approx 0 \quad (36)$$

Nevertheless, under low irradiation intensities, the term $[h^+]^2$ in Eq. (36) can be omitted leading to

$$[h^+] = \frac{k_1}{k_3[OH^-]} I \quad (37)$$

Under high irradiation intensities, where the recombination of electron–hole is predominant, $k_2[h^+]^2 \gg k_3[h^+][OH^-]$. Consequently, $[h^+]$ takes the following form:

$$[h^+] = \left(\frac{k_1}{k_2} I\right)^{1/2} \quad (38)$$

Under high irradiation intensities considering mainly the formation and the recombination of hydroxyl radicals $[OH^\bullet]$ can be obtained using the steady state assumption as below:

$$\frac{d[OH^\bullet]}{dt} = k_3[h^+][OH^-] - 2k_5[OH^\bullet]^2 \approx 0 \quad (39)$$

Consequently, $[OH^\bullet]$ takes the following form:

$$[OH^\bullet] = \sqrt{\left(\frac{k_3}{2k_5}\right)[h^+][OH^-]} \quad (40)$$

The hydroxyl radical concentration $[OH^\bullet]$ can be written introducing the hole concentration $[h^+] = (k_1/k_2)^{1/2} I^{1/2}$ as below:

$$[OH^\bullet] = \sqrt{\left(\frac{k_3}{2k_5}\right)[OH^-]}\left(\frac{k_1}{k_2}\right)^{1/4} I^{1/4} \quad (41)$$

In this case, the photocatalytic degradation rate of the organic compound $r$ is proportional to $I^{1/4}$ explaining the obtained value of kinetic order ($1/4 < n < 1/2$) which is lower than the half-order ($n = 0.5$). Therefore, in this present work, the obtained value of kinetic order ($n = 0.38$) could be attributed to a mixed recombination of electron–hole and hydroxyl radicals in the photocatalytic process. From our point of view, the above original demonstration can supply a solid interpretation concerning the low

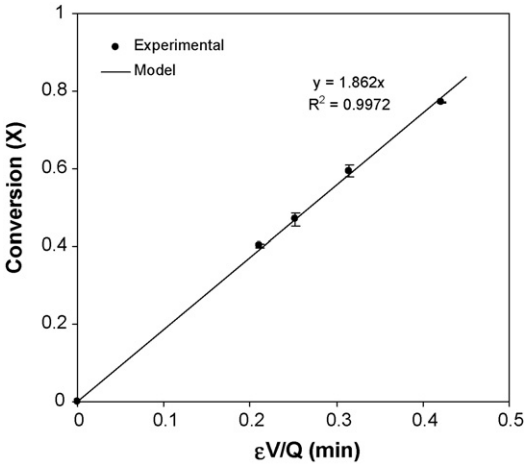


Fig. 13. Effect of contact time on the acetone conversion. Regular conditions used were: incident light irradiance, $\bar{I}_0 = 1.7\,\mathrm{mW\,cm^{-2}}$; relative humidity, RH = 10%; photoreactor temperature, $T_R = 30\,^{\circ}\mathrm{C}$; initial concentration, $C_0 = 1.2\,\mathrm{mg\,L^{-1}}$; oxygen content, air (20 vol% $O_2$).

value ($1/4 < n < 1/2$) without mass transfer limitations. In a previous study, we have found a similar order ($n = 0.34$) for the photocatalytic degradation of methyl ethyl ketone [6].

### 3.5. Effect of contact time

The effect of contact time $\varepsilon V/Q_v$ on the photocatalytic degradation of acetone was investigated in the range of 0.21–0.42 min. It can be noticed that the effect of the contact of the reactant was studied by varying the volumetric flow rate with a constant concentration of acetone. Fig. 13 shows that acetone conversion increased from 0.40 to 0.77 as the contact time increased from 0.21 to 0.42 min (volumetric flow rate decreased from 300 to 150 mL min$^{-1}$). This behaviour has been obtained at high concentration where the rate is independent of concentration (zero-order kinetic). It can be noticed that the photocatalytic degradation rate is independent of contact time (or volumetric flow rate). In our case, the photocatalytic degradation rate was not mass transfer limited (see Section 3.2). When the constants $k_{deg}$ and $K_{LH}$ are determined, it is possible for a given inlet concentration and for a given contact time to calculate the acetone conversion $X$ by solving Eq. (23).

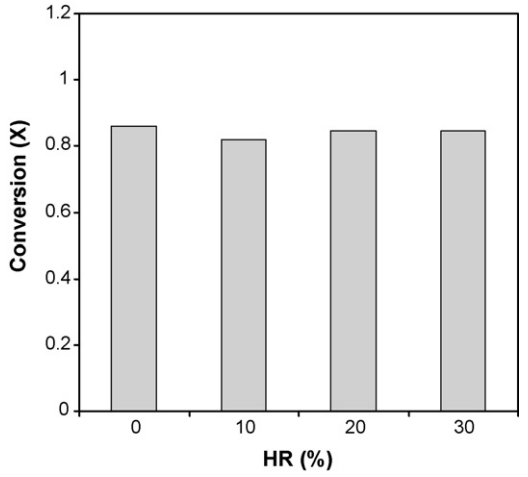


Fig. 14. Effect of water vapour on the acetone conversion. Regular conditions used were: total volume flow rate, $Q_v = 140\,\mathrm{mL\,min^{-1}}$; photoreactor temperature, $T_R = 30\,^{\circ}\mathrm{C}$; incident light irradiance, $\bar{I}_0 = 1.7\,\mathrm{mW\,cm^{-2}}$; initial concentration, $C_0 = 1.2\,\mathrm{mg\,L^{-1}}$.

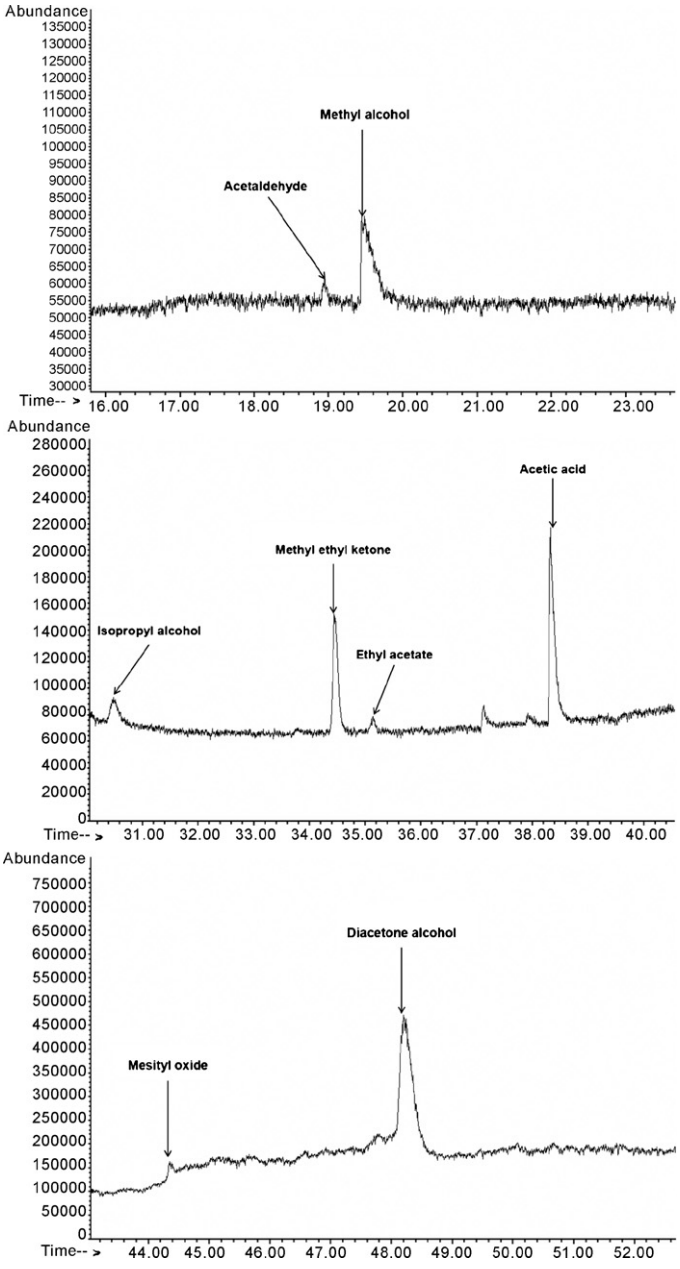


Fig. 15. Typical chromatograms of the effluent obtained by GC/MS after acetone photocatalytic oxidation.

### 3.6. Effect of humidity content

Humidity content is known to significantly influence the photocatalytic oxidation rates and reaction paths [22]. The water molecules can be transformed into hydroxyl radicals ($OH^{\bullet}$) by reacting with the photogenerated holes ($h^+$) at the photocatalyst

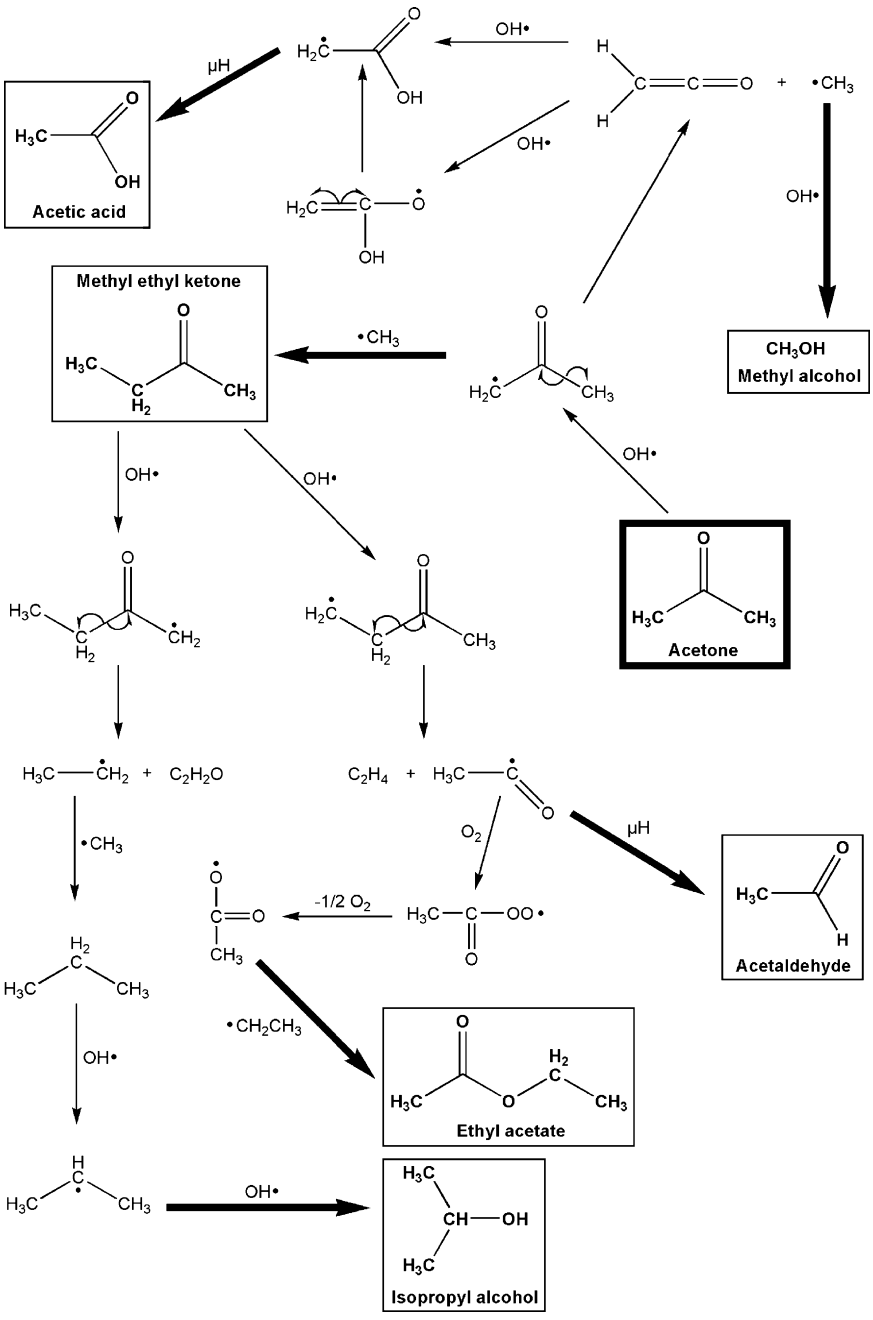


Fig. 16. Photocatalytic degradation pathway of acetone photodegradation on $TiO_2$: chain reactions initiated by $OH^{\bullet}$. Possible formation of methyl alcohol, acetic acid, methyl ethyl ketone, acetaldehyde, ethyl acetate and isopropyl alcohol. The main intermediate products identified by GC/MS are written in bold. Acetone = μH = $H_3C$–CO–$CH_3$.

surface as below:

$$H_2O + h^+ \rightarrow OH^{\bullet} + H^+ \quad (42)$$

The hydroxyl radicals are well known to be strong oxidants and they could enhance the acetone conversion in the presence of the water vapour. However, humidity content could decrease the pollutant conversion due to a possible competitive adsorption between the pollutant and the water molecules. This behaviour has been widely reported by different authors for the photocatalytic oxidation of acetone [14,23]. Kim and Hong [14] have examined the effect of various concentrations of water vapour showing that the addition of water vapour decreases the photocatalytic degradation rate of acetone. Water vapour seems to hinder the adsorption of acetone molecules on the catalyst surface. Furthermore a gradual accumulation of water molecules on the surface of $TiO_2$ can block acetone adsorption sites. In order to examine the effect of humidity content on the acetone conversion, several photocatalytic degradation experiments were investigated at different relative humidity ratio (0–30%). Fig. 14 shows the influence of humidity content on the acetone conversion: an increase of humidity content seems to have no significant effect on the acetone conversion. The same behaviour has been revealed in a previous study on the methyl ethyl ketone (MEK) photocatalytic oxidation [6]. The experimental set-up

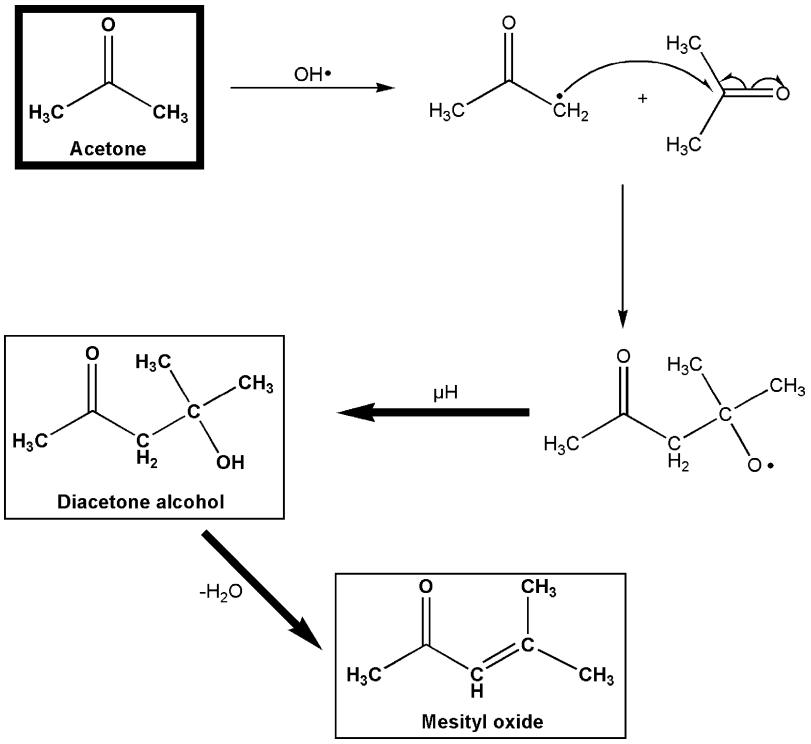


Fig. 17. Photocatalytic degradation pathway of acetone photodegradation on $TiO_2$: chain reactions initiated by $OH^{\bullet}$. Possible formation of diacetone alcohol and mesityl oxide. The main intermediate products identified by GC/MS are written in bold. Acetone = μH = $H_3C$–CO–$CH_3$.

cannot deliver a relative humidity higher than 30% because the water molecules could condense in the experimental set-up and high humidity content could damage the analytical system. Vorontsov et al. [23] have studied the effect of humidity content from 700 to 20,400 ppm on the photocatalytic degradation rate of acetone. They have mentioned a high decrease of degradation rate with humidity content ranging from 700 to 12,500 ppm. In this present work, the effect of humidity content on the acetone conversion was investigated up to 30% corresponding to 13,000 ppm. In this case, the range studied seems to be sufficient in order to highlight a possible competitive adsorption between the pollutant and water molecules.

## 4. By-products of acetone photocatalytic degradation

### 4.1. Identification of acetone by-products

As by-products could be potentially more toxic for the human health than the initial pollutant, identify and quantify them is necessary. It can be noticed that no gaseous intermediates have been detected by FID in the gas phase at the reactor exit suggesting almost total mineralization. However, the used GC/FID apparatus is not equipped with a $CO_x$ detector: the detection and quantification of carbon dioxide cannot be highlighted during the photocatalytic degradation of acetone. Reaction products are condensed in a cool trap placed at the reactor exit. A mixture of ethanol–liquid nitrogen was chosen at a temperature of about −50 °C for 90 min in order to accumulate and identify the minor by-products at the reactor exit. This mixture was chosen to prevent the trap of gaseous oxygen (bp = − 183 °C), which could jam the air flow. The photocatalytic process was realised under dry atmosphere to prevent the trap of water molecules. In a previous study, Vincent et al. [6] have demonstrated that the production of gaseous intermediates seems to be more important under dry atmosphere. After accumulation, a restricted volume of solvent (∼600 μL of pure acetone) has been used in order to recover the trapped by-products. Then the liquid phase was injected into the GC/MS apparatus as described in the Section 2. In this present work, we have identified acetaldehyde, methyl alcohol, isopropyl alcohol, methyl ethyl ketone, ethyl acetate, acetic acid, mesityl oxide and diacetone alcohol, as the main intermediate products in gas phase. Fig. 15 shows the typical chromatogram of the effluent obtained after acetone photocatalytic oxidation. Acetaldehyde, methyl alcohol, isopropyl alcohol, methyl ethyl ketone, ethyl acetate, acetic acid, mesityl oxide and diacetone alcohol were detected at retention times of 18.9, 19.5, 30.5, 34.4, 35.1, 38.3, 44.3 and 48.2 min, respectively. The relative abundance of by-products seems to be in this order: diacetone alcohol > acetic acid > methyl ethyl ketone > methyl alcohol > other by-products. The peaks located at retention times of 37.1 and 37.9 cannot be identified by the MS system. These by-products have very low concentrations and their quantification is impossible. No deactivation phenomenon has been reported during the acetone photocatalytic degradation. It can be noticed that our annular photoreactor is not equipped with a heating system allowing desorption of possible by-products adsorbed at the $TiO_2$ surface. Xu and Raftery [24] have identified diacetone alcohol, mesityl oxide, propylene oxide and acetic acid, as the main intermediate products at the $TiO_2$ surface. Further Coronado et al. [25] have also

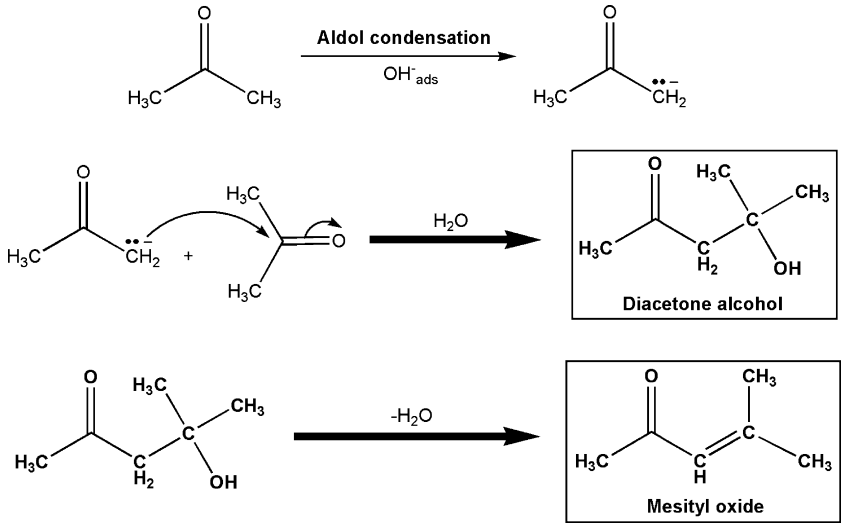


Fig. 18. Photocatalytic degradation pathway of acetone photodegradation on $TiO_2$: aldol condensation. The main intermediate products identified by GC/MS are written in bold.

identified by FTIR spectroscopy acetic acid, acetaldehyde and formic acid, as the possible main by-products at the $TiO_2$ surface.

### 4.2. Mechanism of the acetone photocatalytic degradation

Chain reactions initiated by photogenerated hydroxyl radicals can control the acetone photocatalytic degradation: metathesis, addition, β scission, termination, etc. Upon irradiation, valence band are promoted to the conduction band forming a positive hole behind. The positive holes can oxidize adsorbed water to produce hydroxyl radical. Acetone can react with hydroxyl radical ($OH^{\bullet}$) at the $TiO_2$ surface to form a dimethyl carbonyl radical ($H_2C^{\bullet}–CO–CH_3$) via a metathesis reaction (H-abstraction). This dimethyl carbonyl radical can be decomposed by β scission with a cleavage of C–C bonds in order to produce a methyl radical ($^{\bullet}CH_3$) and ketene ($H_2C{=}C{=}O$) as illustrated in Fig. 16. At low temperature, C–C β scissions are predominant because the C–C binding energy (∼85 kcal $mol^{-1}$) is lower than C–H binding energy (∼100 kcal $mol^{-1}$). The formation of acetic acid can be explained by the reaction of addition between a hydroxyl radical and ketene in order to form $H_2C^{\bullet}–COOH$. This radical can react with acetone (μH) or with $TiO_2$ surface to produce acetic acid. The methyl radical ($^{\bullet}CH_3$) can combine with $OH^{\bullet}$ and $H_2C^{\bullet}–CO–CH_3$ to produce methyl alcohol and methyl ethyl ketone. Guillard [26] has mentioned the possible combination with different alkyl radicals in photocatalysis. In a previous study, it has been demonstrated that acetaldehyde can be formed via the intervention of an ethyl carbonyl radical ($H_3C–^{\bullet}C{=}O$) during the photocatalytic degradation of MEK [6]. Raillard et al. [27] have mentioned the possible formation of esters during the photocatalytic process. The ethyl carbonyl radical can react with molecular oxygen to form the ethyl carbonyl peroxy radical ($H_3C–C(O)OO^{\bullet}$) which can be converted to the acetate radical ($H_3C–C(O)O^{\bullet}$). Ethyl acetate can be ascribed to the reaction between the acetate radical and the ethyl radical (Fig. 16). During the photocatalytic oxidation of MEK, an ethyl radical ($H_2C^{\bullet}–CH_3$) can be produced. This ethyl radical can combine with $^{\bullet}CH_3$ to form propane. Propane can be attacked by hydroxyl radicals to form a propyl radical ($H_3C–HC^{\bullet}–CH_3$) by metathesis, which can combine with $OH^{\bullet}$ in order to produce isopropyl alcohol (Fig. 16).

The dimethyl carbonyl radical ($H_2C^{\bullet}–CO–CH_3$) previously described can be added to acetone to form $H_3C–C(O)–CH_2–C(CH_3)_2–O^{\bullet}$, which can react with μH (acetone) in order to produce diacetone alcohol as illustrated in Fig. 17. Mesityl oxide can be ascribed to the dehydration product of diacetone alcohol.

Diacetone alcohol can be also produced by an aldol condensation (Fig. 18), which is an organic reaction in which an enolate ion reacts with a carbonyl compound to form a β-hydroxyaldehyde or β-hydroxyketone. An enolate ion can be formed by the chemical reaction between acetone and an adsorbed hydroxyl group ($OH^{-}{}_{ads}$) at the photocatalyst surface. Adsorbed hydroxyl groups can be formed by the following reaction:

$$H_2O_{2ads} + O_2{}^{\bullet-}{}_{ads} \rightarrow OH^{\bullet}{}_{ads} + OH^{-}{}_{ads} + O_{2ads} \quad (43)$$

$H_2O_2$ can be generated from $OH^{\bullet}$ and $HO_2{}^{\bullet}$ as follows:

$$2OH^{\bullet}{}_{ads} \rightarrow H_2O_{2ads} \quad (44)$$

$$2HO_2{}^{\bullet}{}_{ads} \rightarrow H_2O_{2ads} + O_{2ads} \quad (45)$$

Mesityl oxide can be ascribed to the dehydration product of diacetone alcohol. The photocatalytic degradation mechanism of acetone seems to be adapted to explain the formation of minor by-products after photocatalytic oxidation. In this present work, we have only proposed a possible mechanism in order to explain the formation of minor by-products in gas phase after accumulation. The minor by-products can be effectively degraded in $CO_2$ in several steps whose reaction pathways still are too complexes to be explicated. Recently Tatsuma et al. [28] have mentioned a possible homogeneous reaction in photocatalysis by diffu-

sion of $OH^{\bullet}$, $HO_2^{\bullet}$ and $H_2O_2$ in the gas phase from the $TiO_2$ surface.

## 5. Conclusion

In this study, the annular photocatalytic reactor has been assimilated to a plug flow reactor. An efficient photocatalytic degradation of acetone on $TiO_2$ P25 Degussa deposited on fibreglass has been observed. No limitation transfer (external and internal limitation) was found under the experimental conditions. The Langmuir–Hinshelwood model has been shown to give a satisfactory fit to the experimental data. The rate of photocatalytic degradation increased with the average incident light irradiance $\bar{I}_0$, being proportional to $\bar{I}_0^{0.38}$. Humidity content seems to have no influence on the rate of acetone degradation. The reaction by-products have been detected by GC/MS after an accumulation into a mixture at $-50\,^{\circ}C$ for 90 min. After intermediates identification, a possible mechanism of acetone photocatalytic degradation has been established in order to explain the formation of the minor by-products.

## Acknowledgement

The authors are indebted to Pr M. Bouchy for his invaluable help in the establishment of the incident light irradiance model and discussions.

## References

[1] D.F. Ollis, C.R. Acad, Sci. II C 3 (2000) 405–411.
[2] H. De Lasa, B. Serrano, M. Salaices, Photocatalytic Reaction Engineering, Springer, New York, 2005.
[3] M. Bouchy, O. Zahraa, Int. J. Photoenergy 5 (2003) 191–197.
[4] NIOSH, Manual of Analytical Methods (NMAM): Method 2555 (2003) 1–5.
[5] N. Doucet, F. Bocquillon, O. Zahraa, M. Bouchy, Chemosphere 65 (2006) 1188–1196.
[6] G. Vincent, A. Queffeulou, P.M. Marquaire, O. Zahraa, J. Photochem. Photobiol. A: Chem. 191 (2007) 42–50.
[7] C. Hachem, F. Bocquillon, O. Zahraa, M. Bouchy, Dyes Pigments 49 (2001) 117–125.
[8] Y. Quan, S.O. Pehkonen, M.B. Ray, Indian Eng. Chem. Res. 43 (2004) 948–955.
[9] Y. Quan, S.O. Pehkonen, M.B. Ray, Indian Eng. Chem. Res. 44 (2005) 3471–3479.
[10] S.M. Ould-Mame, O. Zahraa, M. Bouchy, Int. J. Photoenergy 2 (2000) 59–66.
[11] O. Levenspiel, Chemical Reaction Engineering, John Wiley and Sons, New York, 1999.
[12] J. Villermaux, Génie de la Réaction Chimique, Conception et Fonctionnement des Réacteurs, Lavoisier, Paris, 1993.
[13] O. Carp, C.L. Huisman, A. Reller, Prog. Solid State Chem. 32 (2004) 33–177.
[14] S.B. Kim, S.C. Hong, Appl. Catal. B: Environ. 35 (2002) 305–315.
[15] K.H. Wang, H.H. Tsai, Y.H. Hsieh, Appl. Catal. B: Environ. 17 (1998) 313–320.
[16] W. Wang, Y. Ku, J. Photochem. Photobiol. A: Chem. 159 (2003) 47–59.
[17] W. Choi, J.Y. Ko, H. Park, J.S. Chung, Appl. Catal. B: Environ. 31 (2001) 209–220.
[18] Y. Ohko, K. Hashimoto, A. Fujishima, J. Phys. Chem. A 101 (1997) 8057–8062.
[19] Y. Ohko, A. Fujishima, J. Phys. Chem. B 102 (1998) 1724–1729.
[20] L.C. Chen, T.C. Chou, Indian Eng. Chem. Res. 32 (1993) 1520–1527.
[21] A.G. Rincón, C. Pulgarin, Appl. Catal. B: Environ. 44 (2003) 263–284.
[22] S.B. Kim, H.T. Hwang, S.C. Hong, Chemosphere 48 (2002) 437–444.
[23] A.V. Vorontsov, E.N. Kurkin, E.N. Savinov, J. Catal. 186 (1999) 318–324.
[24] W. Xu, D. Raftery, J. Catal. 204 (2001) 110–117.
[25] J.M. Coronado, S. Kataoka, I. Tejedor-Tejedor, M.A. Anderson, J. Catal. 219 (2003) 219–230.
[26] C. Guillard, J. Photochem. Photobiol. A: Chem. 135 (2000) 65–75.
[27] C. Raillard, V. Héquet, P. Le Cloirec, J. Legrand, Water Sci. Technol. 50 (2004) 241–250.
[28] T. Tatsuma, W. Kubo, A. Fujishima, Langmuir 18 (2002) 9632–9634.